Cation Exchange Reactions in Colloidal Branched Nanocrystals

Karol Miszta, Dirk Dorfs, Alessandro Genovese, Mee Rahn Kim, and Liberato Manna*

Istituto Italiano di Tecnologia, Via Morego 30, 16130 Genova, Italy

ABSTRACT Octapod-shaped colloidal nanocrystals composed of a central "core" region of cubic sphalerite CdSe and pods of hexagonal wurtzite CdS are subject to a cation exchange reaction in which Cd^{2+} ions are progressively exchanged by Cu^{+} ions. The reaction starts from the tip regions of the CdS pods and proceeds toward the center of the nanocrystals. It preserves both the shape and the anionic lattices of the heterostructures. During the exchange, the hexagonal wurtzite CdS pods are converted gradually into pods of hexagonal Cu_2S chalcocite. Therefore, the partial cation exchange reactions lead to the formation of a ternary nanostructure, consisting of an octapod in which the central core is still CdSe, while the pods have a segmented CdS/Cu_2S composition. When the cation exchange reaches the core, the cubic sphalerite CdSe core is converted into a core of cubic $Cu_{2-x}Se$ berzelianite phase. Therefore fully exchanged octapods are composed of a core of $Cu_{2-x}Se$ and eight pods of Cu_2S. All these structures are stable, and the epitaxial interfaces between the various domains are characterized by low lattice mismatch. The $Cu_{2-x}Se$(core)/Cu_2S(pods) octapod represents another example of a nanostructure in which branching is achieved by proper organization of cubic and hexagonal domains in a single nanocrystal.

KEYWORDS: nanocrystals · cation exchange · branched nanostructures · copper sulfide · copper selenide

Branched nanocrystals are gaining increasing interest because of their potential applications in optics,[1] photovoltaics,[2,3] nanomechanics,[4] electronics[5] and sensing.[6] Many synthetic approaches have been developed to them, especially *via* wet chemistry.[7,8] Among the most investigated branched shapes are tetrapods,[9,10] stars,[11] octapods,[12,13] and hyperbranched ones.[14−16] Their synthesis is challenging, due to the presence of byproducts and in general due to the difficulty of achieving a good control over nucleation and growth rates. Advancements in this direction have come from the so-called seeded growth approach,[17−19] where preformed monodisperse seeds with defined habit and crystal phase are injected in the reaction flask together with the precursors of the materials needed to grow the pods. By this approach a fine control is achieved over the synthesis, as the pods are grown only on specific facets of the seeds, the latter becoming the branching regions of the final nanocrystals. Also, the reaction conditions can be set in a way that the growth of pods occurs in a specific crystal phase, while formation of byproducts due to separate nucleation of nanocrystals of the material of the pods can be minimized. The approach has been studied extensively only for a few materials, most of them belonging to the II−VI class of semiconductors.[12,17−19]

Another development in the synthesis of nanocrystals is the exploitation of cation exchange reactions, which are well studied in bulk ionic materials.[20−23] At the nanoscale, different types of cation substitutions have been investigated,[24−30] and they were shown to be an easy and versatile way to obtain a variety of interesting materials.[31−37] During a cation exchange reaction, the sublattice of anions remains in place, while the cation framework is replaced by cations of another chemical species.[38−46] As an example, in both CdS and CdSe nanocrystals, the Cd^{2+} ions can be replaced (in total or in part) by Cu^{+} or by Ag^{+} ions, yielding respectively $Cu_{2-x}Se$, $Cu_{2-x}S$, Ag_2Se, and Ag_2S nanocrystals. These reactions were also shown to be reversible.[43,47] Also CdSe(core)/CdS(shell) rod-shaped nanorods undergo reversible cation exchange with Cu^{+},[38] while preserving their core/shell structure. Cation exchange in nanocrystals was also demonstrated with Pb^{2+} ions as exchanging ions.[38,40] These reactions extend therefore the range of nanocrystals that can be synthesized with controlled shapes and compositions, as one can start from nanocrystals of a material (or combination of materials) for which the synthesis is well established and then convert them into nanocrystals of materials that are accessible *via* a single cation exchange reaction or *via* a sequence of cation exchange reactions, while preserving the original shape.

Our group recently applied both concepts mentioned above and developed a synthetic procedure to obtain octapod-shaped nanocrystals, *via* a two-step approach consisting of (i) cation exchange on cubic berzelianite $Cu_{2-x}Se$ nanocrystals that converted them into sphalerite CdSe nanocrystals and (ii) a seeded growth reaction by which eight CdS pods were grown

* Address correspondence to liberato.manna@iit.it.

Received for review May 30, 2011 and accepted July 28, 2011.

Published online August 02, 2011
10.1021/nn201988w

on top of these freshly formed CdSe seeds. These octapods are therefore composed of a central "core" region of cubic sphalerite CdSe and pods of hexagonal wurtzite CdS (see Scheme 1a).[12] Here we show how cation exchange reaction on these octapods, by which Cd^{2+} ions are progressively exchanged by Cu^{+} ions, yields a series of new nanocrystal heterostructures, depending on the extent of exchange. The reaction starts preferentially at the tip regions of the CdS pods (Scheme 1b) and proceeds toward the branching region of the nanocrystal, while preserving both the shape and the anionic lattices of the octapod. During the exchange, the hexagonal wurtzite phase of the CdS pods is converted gradually into the hexagonal Cu_2S chalcocite phase (Scheme 1c), yielding a ternary structure composed of the central core that is still made of CdSe, while the pods have a segmented composition, with the inner segment (*i.e.*, the one closer to the core) still being CdS and the outer segment being Cu_2S. Finally, the cubic sphalerite CdSe phase of the core is converted into cubic $Cu_{2-x}Se$ berzelianite (Scheme 1d).

Furthermore, the reaction investigated here demonstrates nicely that cation exchange on the nanoscale is able to transform a complex structure made of two different anion lattices into another heterostructure with retention of shape, of both anion lattices and of epitaxial interfaces. It is also interesting to note that in the latter samples the core region, which was the original seed in the synthesis of the octapods, is converted back into berzelianite $Cu_{2-x}Se$, which proves the reversibility of the reaction $Cu_{2-x}Se$(berzelianite) ⇔ CdSe(sphalerite).

All these structures have epitaxial interfaces with low strain. In the ternary CdSe/CdS/Cu_2S octapod, the interface between the CdSe core and the CdS segment of the pod and that between the CdS segment and the Cu_2S segment both have low lattice mismatch. In the fully exchanged octapod, the interface between the hexagonal Cu_2S pod and the cubic $Cu_{2-x}Se$ core has a low lattice mismatch too (about 4%; see Table 1 for details). This octapod is therefore another example of nanostructure in which branching is achieved by a suitable combination of nanoscale domains with two types of crystal phases, namely, a cubic one (berzelianite) and an hexagonal one (chalcocite).

RESULTS AND DISCUSSION

Partial Cation Exchange. Figure 1a is a high-angle annular dark field scanning TEM (HAADF-STEM) image of several octapods from a sample in pristine conditions (*i.e.*, not yet exposed to cation exchange), and Figure 1b is a high-resolution TEM (HRTEM) image of a single pod belonging to a pristine octapod. When small amounts of the Cu^{+} precursor were added to the solution containing octapods (see Table 2, sample number 1 and Experimental Section for details), Cd^{2+} was

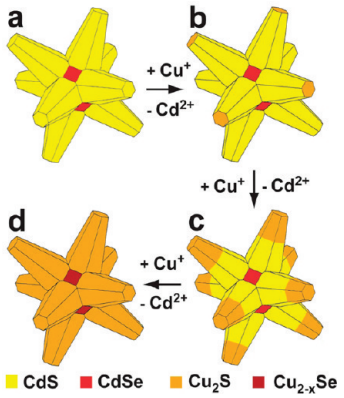

Scheme 1. Series of sketches highlighting the conversion of a CdSe/CdS octapod-shaped nanocrystal (a) to a $Cu_{2-x}Se$/Cu_2S octapod (d) via gradual exchange of Cd^{2+} ions with Cu^{+} ions. The initial and intermediate stages of cation exchange, as depicted in (b) and (c), are certainly idealized in these sketches regarding their concerted evolution. In reality, as explained in the main text, the exchange reaction starts at a different time on each pod. Therefore in an intermediate, partially exchanged octapod, each pod will be characterized by a different extent of exchange.

TABLE 1. Rationalized Lattice Mismatches at CdS//CdSe, CdS//Cu_2S, and Cu_2S//$Cu_{2-x}Se$ Interfaces

	Commensurate Lattice Mismatches *m*					
CdS//CdSe		CdS//Cu_2S		Cu_2S//$Cu_{2-x}Se$	
[0001] // [111]	4.88%	[0001] // [0001]	1.84%	[0001] // [111]	1.27%
$[\bar{1}2\bar{1}0]$ // $[01\bar{1}]$	4.18%	$[\bar{1}2\bar{1}0]$//$[\bar{1}2\bar{1}0]$	3.36%	$[\bar{1}2\bar{1}0]$//$[01\bar{1}]$	3.36%
$[10\bar{1}0]$//2$[2\bar{1}\bar{1}]$	4.14%	$[10\bar{1}0]$//$[10\bar{1}0]$	3.36%	$[10\bar{1}0]$//3$[2\bar{1}\bar{1}]$	3.39%

exchanged with Cu^{+} starting preferentially from the tip regions of the octapods. This could be seen clearly from HRTEM, as shown in Figure 1c. A similar partial cation exchange reaction was already described by Sadtler *et al.*[39] on CdS rods that were progressively transformed into Cu_2S rods, as also in that case the reaction started from the tip regions, which are the most reactive locations in these elongated nanostructures. In our case, each CdS pod has only one tip region exposed, since the opposite side of the pod is blocked by the interface with the central CdSe core. Therefore, the geometry of the octapods is directing a path of cation substitution in the octapods. The apical Cu_2S domains exhibited lattice sets with *d*-spacings that are compatible with the hexagonal Cu_2S chalcocite phase (Figure 1c). At such early stages of cation exchange, often no unique epitaxial relationships could be identified at the tip regions between the CdS pod and the newly formed, small Cu_2S domains. This might be due to the often poorly determined crystal structure at the very tip regions of one-dimensional nanostructures in general, such as the pods in the present case (see HRTEM image of Figure 1b). However, as we shall see in the following, at later stages of the cation exchange a clear epitaxial relationship developed between the

TABLE 2. Amounts of Precursor Used for the Cation Exchange Reaction[a]

sample number	amount of Cu precursor in the sample taken from the stock solution → moles of Cu^+ ions added	methanol	toluene	amount of octapods solution → moles of Cd^{2+}
1	50 μL → 2.68×10^{-7} mol	5 mL	0.5 mL	50 μL → 1.08×10^{-6} mol
2	100μL → 5.3×10^{-7} mol	5 mL	0.5 mL	50 μL→ 1.08×10^{-6} mol
3	250 μL → 1.3×10^{-6} mol	5 mL	0.5 mL	50 μL → 1.08×10^{-6} mol
4	500 μL (excess) → 2.68×10^{-6} mol	5 mL	0.5 mL	50 μL → 1.08×10^{-6} mol
5	2000 μL (excess) → 10.72×10^{-6}mol	5 mL	0.5 mL	50 μL → 1.08×10^{-6} mol

[a] The concentration of Cu^+ ions in the stock solution was 5.3×10^{-3} mol/L.

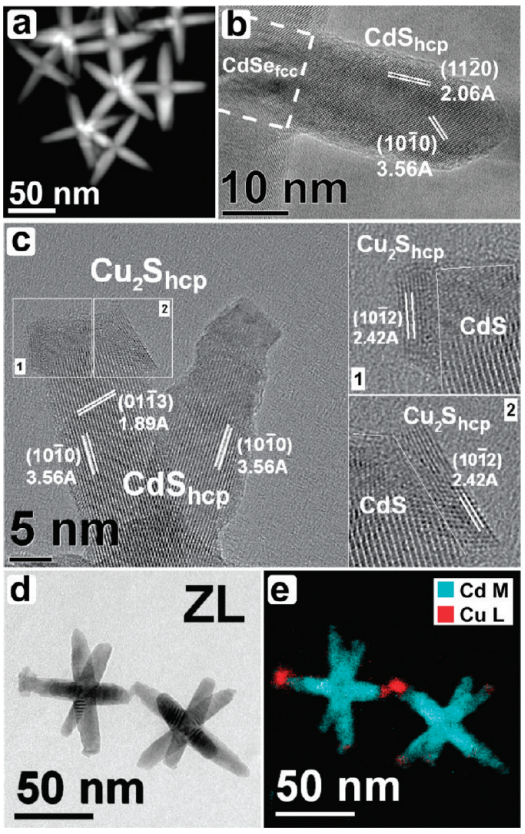

Figure 1. (a) HAADF-STEM image of several pristine octapods. (b) HRTEM image of a pod belonging to a pristine octapod showing the (11$\bar{2}$0) and (10$\bar{1}$0) lattice sets of wurtzite CdS, with *d*-spacings of 2.06 and 3.56 Å, respectively. (c) HRTEM image of two pods belonging to an octapod at the very early stages of cation exchange: the sample underwent exchange of Cd^{2+} with Cu^+ only at the tip regions. Here the (10$\bar{1}$0) and (01$\bar{1}$3) wurtzite CdS lattice sets, with *d*-spacings of 3.56 and 1.89 Å, respectively, are visible. At the tip region of a pod two hcp Cu_2S domains are identifiable. These are highlighted by a square contour and are magnified in the lateral insets. In these small domains, the chalcocite (10$\bar{1}$2) lattice sets with *d*-spacings of 2.42 Å can be seen. (d) Reference elastic filtered (*i.e.*, "zero loss", ZL) image via EFTEM of two octapods, also at the very early stages of Cu ion exchange and (e) corresponding elemental EFTEM map: Cu species are present only at some of the tips.

CdS and the Cu_2S segments in pods of partially exchanged octapods.

Further insights on the extent of cation exchange could be gained from energy filtered TEM (EFTEM). Panels d and e of Figure 1 report an elastic-filtered (zero-loss) image of two octapods and an energy-filtered image of the same octapods. One can see clearly that, while in some pods the process of exchange was well evident at the tips, in other pods only a much smaller fraction of the tip had undergone such exchange, and yet other pods had remained practically unaffected. Therefore, most likely the exchange reactions started at a different time on each pod. This point will be discussed more in detail later.

By further additions of Cu^+ precursor, the phase boundary between chalcocite Cu_2S and wurtzite CdS moved further inward in each pod, while the CdSe core region remained unaffected. Recently, an approach toward single-sided cation exchange on vertically aligned, closed packed CdS nanorods deposited on a substrate was reported.[48] This specific design limited Cd^{2+} to Cu^+ exchange to the top (exposed) part of the rods, while the lower part of the rods was protected by the substrate. Here, the CdS arms of the octapod particles are protected inherently from one side by the CdSe core, therefore providing a similar effect of selectivity but originating exclusively from the morphology of the nanoparticles. As a result, a segmented ternary CdSe (core)/CdS(inner pod section)/Cu_2S(outer pod section) octapod was formed. This could be ascertained both by HRTEM (Figure 2a–c) and by compositional mapping of individual octapods, using both EFTEM and energy dispersive spectroscopy (EDS) (Figure 2d–f). The peculiar shape of the octapod also facilitates TEM analysis. Namely, the octapods have a large central "core" region, and when deposited on a substrate, with four pods often touching the substrate and four pods pointing upward, the core is well exposed and its analysis is straightforward *via* electron microscopy, unlike in the case of tetrapods, where the core is usually hidden behind one of the pods that is pointing straight upward.

In these pods that had undergone not yet complete cation exchange, the CdS section shared epitaxial interfaces with both the CdSe core and the Cu_2S section, as could be seen by the sequence of HRTEM images of Figure 2a–c. Figure 2b is simply a magnified view of the pod region of Figure 2a, where the location of the flat interface between the inner CdS section and the outer Cu_2S section of the pod is marked with two arrows. This interface is even more evident in Figure 2c,

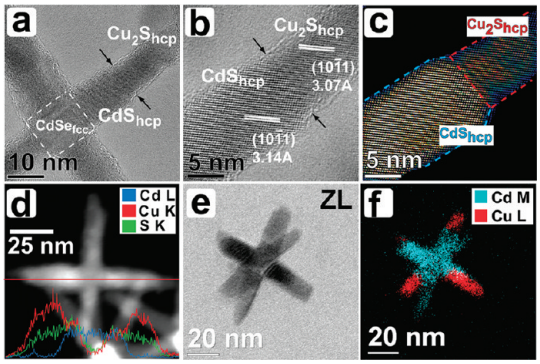

Figure 2. (a) HRTEM image of an octapod after partial exchange of Cd^{2+} with Cu^{+}. In the sample, the CdSe central core is preserved during the exchange reaction; the black arrows indicate the interface between the CdS and the Cu_2S sections along the pod. (b) HRTEM detail of the same pod as in (a), exhibiting the (10$\bar{1}$1) lattice sets (at 3.14 Å) of hcp CdS (inner pod section) and also the (10$\bar{1}$1) lattice sets (at 3.07 Å) of hcp Cu_2S (outer pod section). The interface between the two sections is marked again by black arrows. (c) The corresponding filtered and color-coded image, as described in the text, exhibiting more clearly the distinct CdS and Cu_2S sections and the interface that separates them. The hcp Cu_2S outer pod section has a smaller diameter than the inner CdS pod section and also a smaller unit cell parameter "*a*", as expected for the hcp Cu_2S phase when compared to the hcp CdS phase. (d) HAADF STEM image of a single octapod along with the EDS line profile (horizontal red line) highlighting the variation in the elemental composition along the pods and the core. (e) Reference elastic filtered (ZL) image via EFTEM of a partially cation exchanged octapod and (e) its elemental EFTEM map.

which is a filtered image obtained by the following approach: on two identical FFT images of Figure 2b we applied two masks, in one case to eliminate the wurtzite CdS diffraction spots, in the other case to eliminate the chalcocite Cu_2S diffraction spots. The two inverse-FFT images, obtained from two masked FFT images and labeled with two different colors, were then merged in a single image, *i.e.*, Figure 2c.

Here again, EFTEM analysis (Figure 2f) showed that, while in some pods a considerable section of the pod had undergone cation exchange, in other pods only a much smaller fraction of them or even no fraction at all had undergone such exchange. There are two possible and concomitant reasons for that: (i) the first reason is that, of the eight pods, the tip regions of a group of four pods should be more reactive than the tip regions of the other four pods, given that four pods have crystal polarities that are opposite the crystal polarities of the other four pods;[49] (ii) another reason is that most likely a cation exchange reaction has to overcome an activation barrier at the surface of a nanocrystal in order to get started. Once such a barrier is overcome, exchange proceeds quite quickly through the pod. In the present case, the exchange reaction is more likely to occur at the tips of the pods, where such activation barriers appear to be lower, but even at such tip regions this barrier is not zero, and it should slightly vary from tip to tip. This depends both on what is said in point i and also

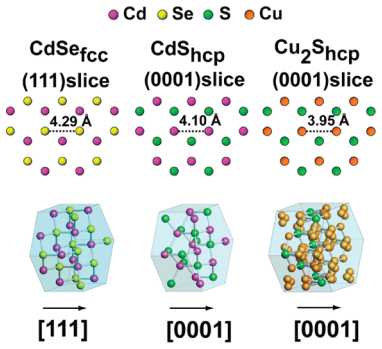

Figure 3. 2D unit cells of CdSe (111), CdS (0001), and Cu_2S (0001) slices and 3D atomic model displaying the stacking of the crystal structures along the growth direction of the pods according to the relative epitaxial rules.

on random conditions, *i.e.*, the degree of surfactant coverage of each specific tip. Therefore, there appears not to be a concerted start in the exchange reaction on all tips, as already discussed in Figure 1, but some tips start getting exchanged before others. Note that in Figure 2f, even though the octapod is tilted, some pods are still partially overlapped, for example the pods on the lower right side. This prevents us from clearly decoupling the extent of cation exchange in each individual pod. This image however is still more informative than for example the EDS map of Figure 2d, in which the octapod being analyzed is sitting on a substrate such that four pods are perfectly overlapped with the other four. Therefore, the corresponding compositional mapping at each point along the scanned line by EDS (except for the central core region) is always a contribution of two overlapping pods.

All interfaces in these "ternary" (*i.e.*, CdSe/CdS/Cu_2S) octapods were epitaxial. The epitaxial relationships characterizing the two types of interfaces are

$$CdS(0002)//CdSe(111)\ \text{and}\ CdS[\bar{1}2\bar{1}0]//CdSe[01\bar{1}] \quad (1)$$

$$Cu_2S(0002)//CdS(0002)\ \text{and}\ Cu_2S[\bar{1}2\bar{1}0]//CdS[\bar{1}2\bar{1}0] \quad (2)$$

In each of these relationships, the first term corresponds to the interface alignment and the second term to the vector alignment. The epitaxial relationships for the two types of interfaces are displayed in Figure 3, where the plan views of the CdSe (111), CdS (0001), and Cu_2S (0001) crystal slices are sketched. It is clear that there are strong similarities in the 2D lattices of the three structures. Figure 3 reports also a 3D atomic model of the stacking of the three crystal structures according to the mentioned epitaxial rules.

Along the interfacial planes CdS (0002)//CdSe (111) and Cu_2S (0002)//CdS (0002) it is possible to calculate the actual lattice mismatches (*m*), defined as the

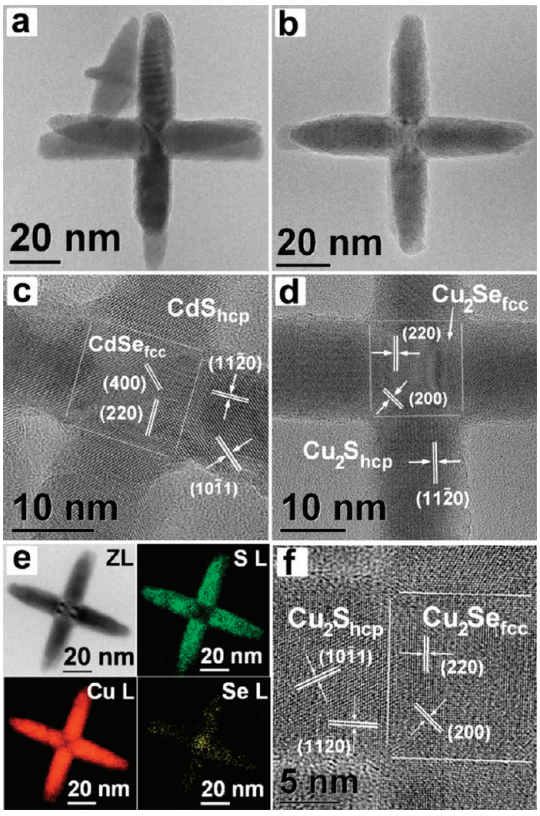

Figure 4. (a) TEM image of a pristine CdSe/CdS octapod; (b) TEM image of a single $Cu_{2-x}Se/Cu_2S$ octapod, as obtained after full cation exchange; (c) HRTEM image of the core/pods region in a CdSe/CdS octapod exhibiting for the core the (400) and (220) CdSe fcc lattice sets with *d*-spacings of 1.52 and 2.15 Å, respectively, and for the pod the (11$\bar{2}$0) and (10$\bar{1}$1) CdS hcp lattice sets with *d*-spacings of 2.06 and 3.14 Å, respectively; (d) HRTEM image of the core/pods region in a $Cu_{2-x}Se/Cu_2S$ octapod, showing for the core the (200) and (220) $Cu_{2-x}Se$ fcc lattice sets with *d*-spacings of 2.88 and 2.03 Å, respectively, and for the pod the (11$\bar{2}$0) Cu_2S hcp lattice set with *d*-spacing of 1.99 Å; (e) Zero-loss (ZL) image and S, Cu, and Se elemental maps of a single $Cu_{2-x}Se/Cu_2S$ octapod acquired by filtering at the S L-edge (165 eV), Cu L-edge (931 eV), and Se L-edge (1436 eV), respectively; (f) HRTEM image of the core/pod region of a $Cu_{2-x}Se/Cu_2S$ octapod where the lattice sets (220) and (200) of the core and (11$\bar{2}$0) and (10$\bar{1}$1) of the pod are visible.

absolute difference between two lattice spacings (d_1 and d_2) along a certain direction, relative to the average of the lattice spacings:

$$m = |d_1 - d_2|/0.5 \times (d_1 + d_2) \quad (3)$$

In particular, as reported in the first two columns of Table 1, the lattice mismatches can be rationalized by considering that in the case of CdS@CdSe epitaxial relationships, one unit cell along the CdSe [111] and CdSe [01$\bar{1}$] directions fits into one unit cell along the CdS [0001] and CdS [$\bar{1}$2$\bar{1}$0] directions, respectively, and three unit cells along the CdSe [2$\bar{1}\bar{1}$] direction fit into one unit cell along the CdS [10$\bar{1}$0] direction. In the case of Cu_2S@CdS epitaxial relationships, one unit cell along the Cu_2S [0001], Cu_2S [$\bar{1}$2$\bar{1}$0], and Cu_2S [10$\bar{1}$0] directions fits into one unit cell along the CdS [0001], CdS [$\bar{1}$2$\bar{1}$0], and CdS [10$\bar{1}$0] directions, respectively. The measured values of the commensurate lattice mismatches are very small along the epitaxial interfaces, revealing therefore a good fit (from the lattice point of view) of the three phases.

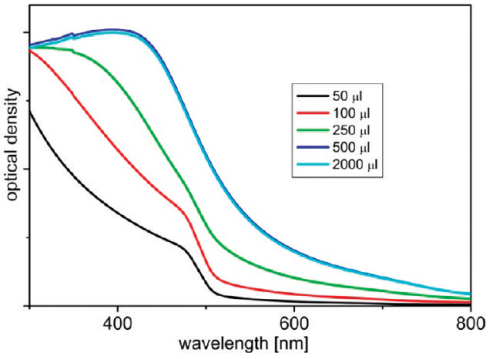

Figure 5. Absorption spectra of a series of partially exchanged octapods. The amount of added volume of a solution of Cu(I) precursor, prepared as described in the Experimental Section, is indicated in the legend. After complete cation exchange, no further variation in the absorption spectra was observed; hence the two spectra with the two highest amounts of added Cu salt (additions of 500 and 2000 μL, respectively) lay on top of each other.

Complete Cation Exchange. When an excess of Cu^+ precursor was used in the cation exchange reaction, the resulting octapods contained only Cu_2S and $Cu_{2-x}Se$ domains, and the shape of the octapod nanocrystals was preserved; see Figure 4 (panels a and c show again a pristine CdSe/CdS octapod; panel b and d show a $Cu_{2-x}Se/Cu_2S$ octapod). A small difference in size between the two structures was observed and is caused by the difference in lattice parameters between the Cd- and the Cu-based components. Crystal structure analyses obtained through HRTEM data (Figure 4c, d) confirmed that, while the original octapods have a sphalerite (fcc) CdSe core and wurtzite (hcp) CdS pods, the octapods after cation exchange consist of a berzelianite (fcc) $Cu_{2-x}Se$ core and chalcocite (hcp) Cu_2S pods. Hence, the anion lattice is conserved during the cation exchange procedure for the fcc core as well as for the hcp pods. EFTEM elemental analysis of the resulting octapods confirmed the findings from HRTEM analysis (see Figure 4e). While Cu was found all over the structure, S was found only in the pods and not in the core of the octapods, and Se instead was found mainly in the core, with a tiny halo also in the pods. Furthermore, it is important to notice that, since the Cu_2S phase replaces the CdS but preserves its crystallographic orientation, after complete Cu^+ exchange the Cu_2S pods and the $Cu_{2-x}Se$ cores exhibit the same epitaxial relationships as those between the previous CdS pods and CdSe cores, namely,

$$Cu_2S(0002)//Cu_{2-x}Se(111) \text{ and } Cu_2S[\bar{1}2\bar{1}0]//Cu_{2-x}Se[01\bar{1}] \quad (4)$$

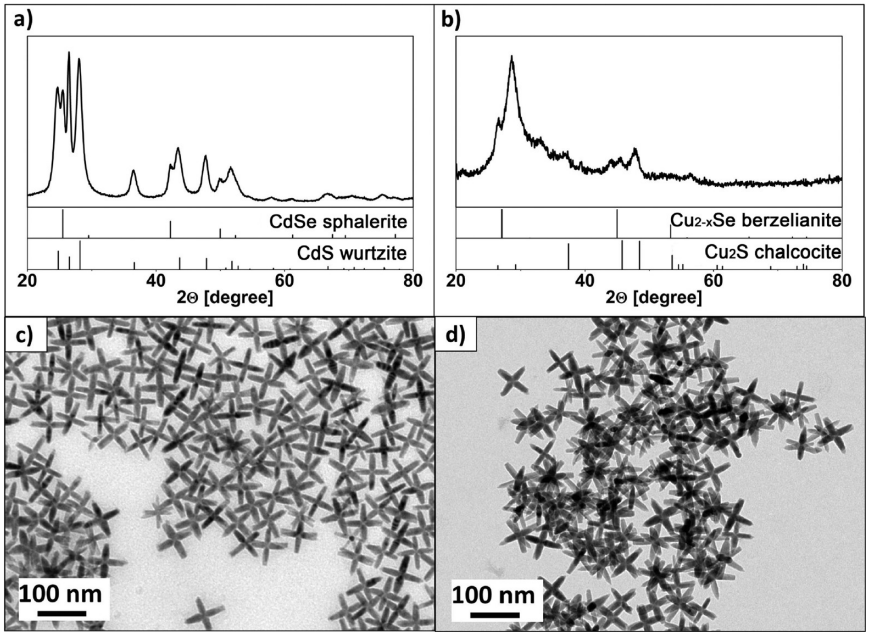

Figure 6. (a) X-ray diffraction of the pristine CdSe/CdS octapods (*i.e.*, before cation exchange) and (b) X-ray diffraction of $Cu_{2-x}Se/Cu_2S$ octapods (*i.e.*, after complete cation exchange); (c) survey TEM image of CdSe/CdS octapods before cation exchange and (d) survey TEM image of the corresponding $Cu_{2-x}Se/Cu_2S$ octapods.

Here again low values of lattice mismatch are found at the interface between the two new phases (see Table 1, last column).

The cation exchange process could also be followed optically, by recording absorption spectra of aliquots collected from the reaction flask (see also Table 2 for amounts of precursors used). During the stepwise partial cation exchange of the CdSe/CdS octapods to $Cu_{2-x}Se/Cu_2S$ octapods, the absorption shoulder at around 475 nm disappeared gradually, due to the smaller and smaller contribution from CdS in the system, which was being transformed into Cu_2S. At the same time, the overall absorption spectrum increased in intensity and a new (unstructured) absorption arose between 600 and 700 nm, which could be assigned to the increasing volume of Cu_2S in the sample. Once full ion exchange was realized, no more change in the absorption spectrum was observed even when larger amounts of Cu salt were added to the solution (Figure 5).

Figure 6 reports the X-ray diffraction patterns of a sample of pristine octapods (a) and of the octapods after complete cation exchange (b). The diffraction pattern of the pristine sample could be easily identified as arising from contributions by both sphalerite CdSe and wurtzite CdS. After cation exchange the X-ray pattern could be assigned mainly to the berzelianite (cubic) phase of $Cu_{2-x}Se$ and the chalcocite phase of Cu_2S. It should be noted however that the overall X-ray scattering intensity of this sample was much lower than that of the pristine sample. We attribute this to the fact that for Cu_2S there are various possibilities for the Cu^+ ions to be distributed within the anion lattice. Thus, most likely after cation exchange a large variety of cation sites were occupied, which resulted in a considerable disorder of the cation lattice and therefore in an overall smaller X-ray scattering intensity. Therefore, X-ray diffraction alone does not really allow distinguishing between the low-temperature monoclinic modification and the high-temperature hexagonal modification of chalcocite. Nevertheless, by combining XRD data with HR-TEM data we could conclude that the hexagonal modification of Cu_2S was formed. This is interesting by itself, as this modification is known to be metastable at room temperature.[50] Thus, this finding represents an example of a cation exchange reaction on nanoparticles that yields materials and modifications that are not accessible by other routes at the given conditions, but which become accessible by cation exchange thanks to anion lattice retention.

CONCLUSIONS

We have reported the synthesis of octapod-shaped $Cu_{2-x}Se/Cu_2S$ nanocrystals *via* cation exchange starting from CdSe/CdS octapods. In the process, the anion lattices of both the hcp pods and the fcc core of the structure are conserved. The exchange starts preferentially from the tips of the octapods, then the phase boundary between Cu_2S and CdS in the pods moves progressively toward the center of the octapod upon addition of increasing amounts of the Cu(I) precursor, while the CdSe sphalerite core remains untouched. At last, also the CdSe core is transformed into $Cu_{2-x}Se$. Our results demonstrate that the anion lattices and also the epitaxial relationships are retained upon cation exchange. These octapods are also very uniform in shape distribution and therefore, in addition to being

appealing for photovoltaics and nanoelectronics, can be interesting candidates for studying mechanical properties at the nanoscale. Since the shape is preserved during cation exchange, these tests could reveal valuable material-related data on elastic and plastic behavior at the nanoscale.

EXPERIMENTAL SECTION

Synthesis of the Octapod CdSe(core)/CdS(pods) Nanocrystals. The synthesis of the berzelianite $Cu_{2-x}Se$ nanocrystal seeds, as well as the synthesis of CdSe/CdS octapods was carried out according to procedures reported by our group.[12,51]

Cation Exchange of CdSe (core)/CdS(pods) Octapods. Cu^+ ion exchange was performed in an argon-filled glovebox. In a standard procedure, a stock solution of Cu^+ ion precursor was prepared by dissolving 10 mg of Cu precursor (tetrakisacetonitrilecopper(I) hexafluorophosphate) in 5 mL of methanol. The reaction vials contained 5 mL of methanol and 0.5 mL of toluene. Subsequently, fixed amounts (see Table 2) of copper(I) precursor were added into these vials. In the last step, 50 μL of a solution of octapods dissolved in toluene was injected into each of these vials (the concentration of the octapods in the solution was 1.2×10^{-7}, with a total Cd concentration equal to 2.17×10^{-2} mol/L). All these reactions were carried out at room temperature. When a smaller amount of copper(I) precursor was used, the final color of the solution was dark yellow, while in the vials with a larger amount of Cu^+ ions added the color of the solution changed rapidly from yellow to brown. In the case of excess amounts of Cu^+ ions added, the cation exchange reaction was complete. In all experiments, the change in color was practically instantaneous, indicating that the cation exchange is a fast process, as found already by many previous reports. However, after injection we left the solution untouched for 5 min, after which the nanocrystals were precipitated by centrifugation and were then redissolved in chloroform.

Characterization. Conventional transmission electron microscopy images were recorded on a JEOL JEM 1011 microscope operating at 100 kV. High-resolution TEM (HRTEM), high-angular annular dark field scanning TEM (STEM), and energy filtered TEM (EFTEM) measurements were performed with a JEOL JEM-2200FS microscope, equipped with a field emission gun working at an accelerating voltage of 200 kV, a CEOS spherical aberration corrector objective lens allowing to reach a spatial resolution of 0.9 Å, and an "in-column" Omega filter. The chemical composition of single particles was determined by energy dispersive X-ray spectroscopy analysis performed in STEM mode, with a JED-2300 Si(Li) detector, using an electron probe of 0.7 Å. Elemental maps *via* EFTEM were acquired using a contrast aperture of about 10 mrad to reduce aberrations, mostly chromatic, and using the three-window method (one post- and two pre-edge) to extract the background. The elastic image (or zero-loss image) was acquired as reference with a 10 eV wide energy slit; then, elemental maps using the S L-edge (165 eV), Cu L-edge (931 eV), Cd M-edge (404 eV), and Se L-edge (1436 eV) were acquired on the same area of zero-loss with energy slits of 20, 50, 30, and 60 eV, respectively. Powder X-ray diffraction measurements were performed with a Rigaku SmartLab X-ray diffractometer. Concentrated nanocrystal solutions were spread on top of a silicon miscut substrate, after which the sample was allowed to dry and was then measured in parallel beam reflection geometry theta/2theta. Optical absorption measurements were carried out using a Varian Cary 5000 UV–vis–NIR spectrophotometer and 1 cm quartz cuvettes. Nanocrystals were dispersed in trichloroethylene (Sigma-Aldrich, spectroscopic grade) for this purpose. Elemental analysis on octapod solutions was carried out *via* Inductively Coupled Plasma Atomic Emission Spectroscopy (ICP-AES). Samples were dissolved in HCl/HNO_3 3:1 (v/v).

Acknowledgment. The authors acknowledge financial support from the European Union through the FP7 starting ERC grant NANO-ARCH (contract number 240111).

REFERENCES AND NOTES

1. Talapin, D. V.; Lee, J.-S.; Kovalenko, M. V.; Shevchenko, E. V. Prospects of Colloidal Nanocrystals for Electronic and Optoelectronic Applications. *Chem. Rev.* **2009**, *110*, 389–458.
2. Goodman, M. D.; Zhao, L.; DeRocher, K. A.; Wang, J.; Mallapragada, S. K.; Lin, Z. Self-Assembly of CdTe Tetrapods into Network Monolayers at the Air/Water Interface. *ACS Nano* **2010**, *4*, 2043–2050.
3. Zhong, H.; Zhou, Y.; Yang, Y.; Yang, C.; Li, Y. Synthesis of Type II CdTe–CdSe Nanocrystal Heterostructured Multiple-Branched Rods and Their Photovoltaic Applications. *J. Phys. Chem. C* **2007**, *111*, 6538–6543.
4. Choi, C. L.; Koski, K. J.; Sivasankar, S.; Alivisatos, A. P. Strain-Dependent Photoluminescence Behavior of CdSe/CdS Nanocrystals with Spherical, Linear, and Branched Topologies. *Nano Lett.* **2009**, *9*, 3544–3549.
5. Fang, L.; Park, J. Y.; Cui, Y.; Alivisatos, P.; Shcrier, J.; Lee, B.; Wang, L.-W.; Salmeron, M. Mechanical and Electrical Properties of CdTe Tetrapods Studied by Atomic Force Microscopy. *J. Chem. Phys.* **2007**, *127*, 184704.
6. Calestani, D.; Zha, M.; Mosca, R.; Zappettini, A.; Carotta, M. C.; Di Natale, V.; Zanotti, L. Growth of ZnO Tetrapods for Nanostructure-Based Gas Sensors. *Sens. Actuators, B* **2010**, *144*, 472–478.
7. Yang, Y.; Jin, Y.; He, H.; Wang, Q.; Tu, Y.; Lu, H.; Ye, Z. Dopant-Induced Shape Evolution of Colloidal Nanocrystals: The Case of Zinc Oxide. *J. Am. Chem. Soc.* **2010**, *132*, 13381–13394.
8. Alivisatos, A. P. Semiconductor Clusters, Nanocrystals, and Quantum Dots. *Science* **1996**, *271*, 933–937.
9. Manna, L.; Milliron, D. J.; Meisel, A.; Scher, E. C.; Alivisatos, A. P. Controlled Growth of Tetrapod-Branched Inorganic Nanocrystals. *Nat. Mater.* **2003**, *2*, 382–385.
10. Fu, W.; Qin, S.; Liu, L.; Kim, T.-H.; Hellstrom, S.; Wang, W.; Liang, W.; Bai, X.; Li, A.-P.; Wang, E. Ferroelectric Gated Electrical Transport in CdS Nanotetrapods. *Nano Lett.* **2011**, *11*, 1913–1918.
11. Huang, T.; Zhao, Q. A.; Xiao, J. Y.; Qi, L. M. Controllable Self-Assembly of PbS Nanostars into Ordered Structures: Close-Packed Arrays and Patterned Arrays. *ACS Nano* **2010**, *4*, 4707–4716.
12. Deka, S.; Miszta, K.; Dorfs, D.; Genovese, A.; Bertoni, G.; Manna, L. Octapod-Shaped Colloidal Nanocrystals of Cadmium Chalcogenides *via* "One-Pot" Cation Exchange and Seeded Growth. *Nano Lett.* **2010**, *10*, 3770–3776.
13. Huang, X.; Zhao, Z.; Fan, J.; Tan, Y.; Zheng, N. Amine-Assisted Synthesis of Concave Polyhedral Platinum Nanocrystals Having {411} High-Index Facets. *J. Am. Chem. Soc.* **2011**, *133*, 4718–4721.
14. Kanaras, A. G.; Sonnichsen, C.; Liu, H. T.; Alivisatos, A. P. Controlled Synthesis of Hyperbranched inOrganic Nanocrystals with Rich Three-Dimensional Structures. *Nano Lett.* **2005**, *5*, 2164–2167.
15. Zhang, H. T.; Ha, D. H.; Hovden, R.; Kourkoutis, L. F.; Robinson, R. D. Controlled Synthesis of Uniform Cobalt Phosphide Hyperbranched Nanocrystals Using Tri-*n*-Octylphosphine Oxide as a Phosphorus Source. *Nano Lett.* **2011**, *11*, 188–197.
16. Amirav, L.; Lifshitz, E. Spray-Produced Coral-Shaped Assemblies of MnS Nanocrystal Clusters. *J. Phys. Chem. B* **2006**, *110*, 20922–20926.

17. Carbone, L.; Nobile, C.; De Giorgi, M.; Sala, F. D.; Morello, G.; Pompa, P.; Hytch, M.; Snoeck, E.; Fiore, A.; Franchini, I. R.; *et al*. Synthesis and Micrometer-Scale Assembly of Colloidal CdSe/CdS Nanorods Prepared by a Seeded Growth Approach. *Nano Lett.* **2007**, *7*, 2942–2950.
18. Talapin, D. V.; Koeppe, R.; Gotzinger, S.; Kornowski, A.; Lupton, J. M.; Rogach, A. L.; Benson, O.; Feldmann, J.; Weller, H. Highly Emissive Colloidal CdSe/CdS Heterostructures of Mixed Dimensionality. *Nano Lett.* **2003**, *3*, 1677–1681.
19. Fiore, A.; Mastria, R.; Lupo, M. G.; Lanzani, G.; Giannini, C.; Carlino, E.; Morello, G.; De Giorgi, M.; Li, Y.; Cingolani, R.; *et al*. Tetrapod-Shaped Colloidal Nanocrystals of II-VI Semiconductors Prepared by Seeded Growth. *J. Am. Chem. Soc.* **2009**, *131*, 2274–2282.
20. Estrada, C. A.; Zingaro, R. A.; Meyers, E. A.; Nair, P. K.; Nair, M. T. S. Modification of Chemically Deposited ZnSe Thin Films by Ion Exchange Reaction with Copper Ions in Solution. *Thin Solid Films* **1994**, *247*, 208–212.
21. Ristova, M.; Ristov, M. XPS Profile Analysis on CdS Thin Film Modified with Ag by an Ion Exchange. *Adv. Surf. Sci.* **2001**, *181*, 68–77.
22. Ristova, M.; Ristov, M.; Tosev, P.; Mitreski, M. Silver Doping of Thin CdS Films by an Ion Exchange Process. *Thin Solid Films* **1998**, *315*, 301–304.
23. Yu, J.; Zhang, J.; Jaroniec, M. Preparation and Enhanced Visible-Light Photocatalytic H_2-Production Activity of CdS Quantum Dots-Sensitized $Zn_{1-x}Cd_xS$ Solid Solution. *Green Chem.* **2010**, *12*, 1611–1614.
24. Moon, G. D.; Ko, S.; Xia, Y.; Jeong, U. Chemical Transformations in Ultrathin Chalcogenide Nanowires. *ACS Nano* **2010**, *4*, 2307–2319.
25. Ethayaraja, M.; Bandyopadhyaya, R. Model for Core−Shell Nanoparticle Formation by Ion-Exchange Mechanism. *Ind. Eng. Chem. Res.* **2008**, *47*, 5982–5985.
26. Yu, J.; Zhang, J.; Liu, S. Ion-Exchange Synthesis and Enhanced Visible-Light Photoactivity of CuS/ZnS Nanocomposite Hollow Spheres. *J. Phys. Chem. C* **2010**, *114*, 13642–13649.
27. Zhang, B.; Jung, Y.; Chung, H.-S.; Vugt, L. V.; Agarwal, R. Nanowire Transformation by Size-Dependent Cation Exchange Reactions. *Nano Lett.* **2009**, *10*, 149–155.
28. Wark, S. E.; Hsia, C.-H.; Son, D. H. Effects of Ion Solvation and Volume Change of Reaction on the Equilibrium and Morphology in Cation-Exchange Reaction of Nanocrystals. *J. Am. Chem. Soc.* **2008**, *130*, 9550–9555.
29. Jeong, U.; Kim, J. U.; Xia, Y. N. Monodispersed Spherical Colloids of Se@CdSe: Synthesis and Use as Building Blocks in Fabricating Photonic Crystals. *Nano Lett.* **2005**, *5*, 937–942.
30. Dong, C.; van Veggel, F. C. J. M. Cation Exchange in Lanthanide Fluoride Nanoparticles. *ACS Nano* **2008**, *3*, 123–130.
31. Kovalenko, M. V.; Talapin, D. V.; Loi, M. A.; Cordella, F.; Hesser, G.; Bodnarchuk, M. I.; Heiss, W. Quasi-Seeded Growth of Ligand-Tailored PbSe Nanocrystals Through Cation-Exchange-Mediated Nucleation. *Angew. Chem., Int. Ed.* **2008**, *47*, 3029–3033.
32. Dorn, A.; Allen, P. M.; Harris, D. K.; Bawendi, M. G. In Situ Electrical Monitoring of Cation Exchange in Nanowires. *Nano Lett.* **2010**, *10*, 3948–3951.
33. Song, J. H.; Messer, B.; Wu, Y. Y.; Kind, H.; Yang, P. D. MMo_3Se_3 ($M = Li^+$, Na^+, Rb^+, Cs^+, NMe^{4+}) Nanowire Formation *via* Cation Exchange in Organic Solution. *J. Am. Chem. Soc.* **2001**, *123*, 9714–9715.
34. Dloczik, L.; Koenenkamp, R. Nanostructured Metal Sulfide Surfaces by Ion Exchange Processes. *J. Solid State Electrochem.* **2004**, *8*, 142–146.
35. Smith, A. M.; Nie, S. M. Bright and Compact Alloyed Quantum Dots with Broadly Tunable Near-Infrared Absorption and Fluorescence Spectra through Mercury Cation Exchange. *J. Am. Chem. Soc.* **2011**, *133*, 24–26.
36. Regulacio, M. D.; Ye, C.; Lim, S. H.; Bosman, M.; Polavarapu, L.; Koh, W. L.; Zhang, J.; Xu, Q. H.; Han, M. Y. One-Pot Synthesis of $Cu_{1.94}S$-CdS and $Cu_{1.94}S$-$ZnxCd_{1-x}S$ Nanodisk Heterostructures. *J. Am. Chem. Soc.* **2011**, *133*, 2052–2055.
37. Matsuda, T.; Kim, J.; Moritomo, Y. Symmetry Switch of Cobalt Ferrocyanide Framework by Alkaline Cation Exchange. *J. Am. Chem. Soc.* **2010**, *132*, 12206–12207.
38. Jain, P. K.; Amirav, L.; Aloni, S.; Alivisatos, A. P. Nanoheterostructure Cation Exchange: Anionic Framework Conservation. *J. Am. Chem. Soc.* **2010**, *132*, 9997–9999.
39. Sadtler, B.; Demchenko, D. O.; Zheng, H.; Hughes, S. M.; Merkle, M. G.; Dahmen, U.; Wang, L. W.; Alivisatos, A. P. Selective Facet Reactivity during Cation Exchange in Cadmium Sulfide Nanorods. *J. Am. Chem. Soc.* **2009**, *131*, 5285–5293.
40. Lambert, K.; De Geyter, B.; Moreels, I.; Hens, Z. PbTeICdTe CorelShell Particles by Cation Exchange, a HR-TEM Study. *Chem. Mater.* **2009**, *21*, 778–780.
41. Chen, W. H.; Yang, Y. F.; Shao, H. X.; Fan, J. Tunable Electrochemical Properties Brought About by Partial Cation Exchange in Hydrotalcite-Like Ni-Co/Co-Ni Hydroxide Nanosheets. *J. Phys. Chem. C* **2008**, *112*, 17471–17477.
42. Zhong, X. H.; Feng, Y. Y.; Zhang, Y. L.; Gu, Z. Y.; Zou, L. A Facile Route to Violet- to Orange-Emitting $Cd_xZn_{1-x}Se$ Alloy Nanocrystals *via* Cation Exchange Reaction. *Nanotechnology* **2007**, 18.
43. Robinson, R. D.; Sadtler, B.; Demchenko, D. O.; Erdonmez, C. K.; Wang, L. W.; Alivisatos, A. P. Spontaneous Superlattice Formation in Nanorods through Partial Cation Exchange. *Science* **2007**, *317*, 355–358.
44. Chan, E. M.; Marcus, M. A.; Fakra, S.; ElNaggar, M.; Mathies, R. A.; Alivisatos, A. P. Millisecond Kinetics of Nanocrystal Cation Exchange Using Microfluidic X-ray Absorption Spectroscopy. *J. Phys. Chem. A* **2007**, *111*, 12210–12215.
45. Camargo, P. H. C.; Lee, Y. H.; Jeong, U.; Zou, Z. Q.; Xia, Y. N. Cation Exchange: A Simple and Versatile Route to Inorganic Colloidal Spheres with the Same Size but Different Compositions and Properties. *Langmuir* **2007**, *23*, 2985–2992.
46. Son, D. H.; Hughes, S. M.; Yin, Y. D.; Alivisatos, A. P. Cation Exchange Reactions in Ionic Nanocrystals. *Science* **2004**, *306*, 1009–1012.
47. Lubeck, C. R.; Han, T. Y. J.; Gash, A. E.; Satcher, J. H.; Doyle, F. M. Synthesis of Mesostructured Copper Sulfide by Cation Exchange and Liquid-Crystal Templating. *Adv. Mater.* **2006**, *18*, 781–748.
48. Rivest, J. B.; Swisher, S. L.; Fong, L.-K.; Zheng, H.; Alivisatos, A. P. Assembled Monolayer Nanorod Heterojunctions. *ACS Nano* **2011**, *5*, 3811–3816.
49. Manna, L. Wang; Cingolani, R.; Alivisatos, A. P., First-Principles Modeling of Unpassivated and Surfactant-Passivated Bulk Facets of Wurtzite CdSe: A Model System for Studying the Anisotropic Growth of CdSe Nanocrystals. *J. Phys. Chem. B* **2005**, *109*, 6183–6192.
50. Kashida, S.; Shimosaka, W.; Mori, M.; Yoshimura, D. Valence Band Photoemission Study of the Copper Chalcogenide Compounds, Cu_2S, Cu_2Se and Cu_2Te. *J. Phys. Chem. Solids* **2003**, *64*, 2357–2363.
51. Deka, S.; Genovese, A.; Yang, Z.; Miszta, K.; Bertoni, G.; Krahne, R.; Giannini, C.; Manna, L. Phosphine-Free Synthesis of p-Type Copper(I) Selenide Nanocrystals in Hot Coordinating Solvents. *J. Am. Chem. Soc.* **2010**, *132*, 8912–8914.